Silicon Nanoparticles: Excitonic Fine Structure and Oscillator Strength

Cedrik Meier[1], Stephan Lüttjohann[1], Matthias Offer[1], Hartmut Wiggers[2], and Axel Lorke[1]

[1] Department of Physics and CeNIDE, University of Duisburg-Essen, Lotharstr. 1, 47057 Duisburg, Germany
cedrik.meier@uni-due.de
[2] Combustion & Gas Dynamics and CeNIDE, University of Duisburg-Essen, Lotharstr. 1, 47057 Duisburg, Germany

Abstract. In this review, recent results on optical spectroscopy on silicon nanoparticles are summarized. We will demonstrate the quantum size effect observed in the photoluminescence for nanoparticles with diameters below 10 nm. Moreover, the excitonic fine structure splitting caused by the exchange interaction is investigated using time-resolved and magnetic-field-dependent photoluminescence measurements. From these results, it is possible to estimate the rate of non-radiative recombinations in these nanoparticles, which allows to determine the oscillator strength and the quantum yield independently.

1 Introduction

Silicon has in the past been the most important material for modern microelectronics. In the last two decades, however, interest in nanostructured silicon has increased significantly. This development is on the one hand triggered by the ongoing miniaturization of silicon based integrated circuits for electronic applications, where critical dimensions $CD < 100\,\mathrm{nm}$ can be reached in large scale production processes. On the other hand, the finding of photoluminescence in porous silicon [1] has sparked the hope for silicon as a material also for optoelectronic applications. Until today, photoluminescence from nanostructured silicon could be demonstrated not only from porous silicon, but also silicon nanocrystals formed in an SiO_2 matrix by implantation of Si ions and subsequent annealing [2–4] and isolated silicon nanoparticles [5–8]. Recently, in silicon nanocrystal based devices amplified stimulated emission [9] and field-injection based electroluminescence [10] could be demonstrated.

As an important prerequesite for optoelectronic device applications, one needs to have detailed knowledge of the recombination dynamics. In the case of silicon nanoparticles, this is of special importance, as bulk silicon is an indirect

semiconductor and only shows vanishing near band-edge photoluminescencence. In this paper, we will review results obtained on the size-dependence of the photoluminescence, the recombination dynamics, which can be explained using the excitonic fine structure, and on the oscillator strength of the radiative recombinations in these systems.

2 Experimental details

All the results presented here have been obtained using Si nanoparticles fabricated in a low-pressure microwave plasma using silane (SiH_4) as a precursor gas. Details of the fabrication process can be found in [11]. The photoluminescence measurements have been performed under excitation from a 532 nm laser in continuous operation in a confocal photoluminescence setup using a Czerny-Turner monochromator and a liquid-nitrogen-cooled charge-coupled device. For the time-resolved photoluminescence measurements, an acousto-optical modulator in combination with an avalanche photodiode was used. The time resolution of this setup is in the range of 4 ns.

3 Results and discussion

In Fig. 1, the room temperature photoluminescence of a bulk silicon sample and silicon nanoparticles with $d \approx 4.5$ nm are shown. From these spectra, one can make the following observations: First, the photoluminescence emission from the bulk silicon sample is significantly sharper than the emission from the silicon nanoparticle sample. The full width of half maximum (FWHM) of the Si bulk sample is $\Delta E \approx 120$ meV, while the Si nanoparticles show a FWHM of about $\Delta E \approx 400$ meV. This spectral broadening is caused by the size distribution of the silicon nanoparticles, which is intrinsic to the fabrication procedure [11]. The second noteworthy fact is the spectral shift in the Si nanoparticle emission towards higher energies compared to the Si bulk sample. This is a consequence of the quantum size effect typically observed in nanocrystalline Si samples. The final observation is related to the photoluminescence intensity. Taking into account the spectral response of the different detectors and the influence of the other optical components (instrument function) and the acquisition time, one finds that the intensity of the photoluminescence emission of the Si nanoparticle sample is about 1500× higher than that of the Si bulk sample. The increase in photoluminescence intensity with respect to the bulk is due to the stronger localization of electrons and holes inside the nanoparticles rather than due to a transition from an indirect semiconductor to a direct semiconductor as was predicted theoretically for small particle diameters [12]. For particles with diameters larger than $d = 2.0$ nm, the Si nanoparticles remain indirect semiconductors, as could be verified by time-resolved photoluminescence and absorption measurements [7].

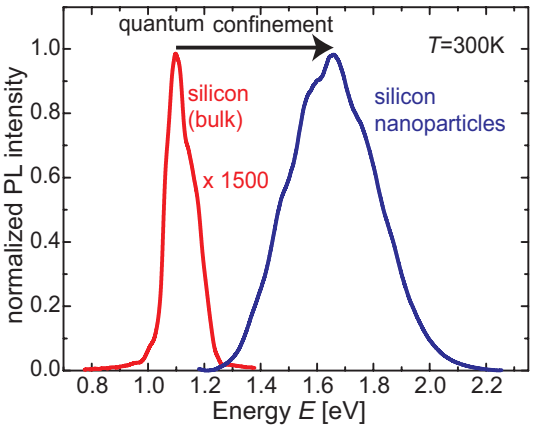

Fig. 1. Room temperature photoluminescence of bulk silicon and silicon nanoparticles.

As mentioned above, the reason for the blue-shift of the PL emission energy is the quantum size effect observed in the Si nanoparticles. The true origin of this is still under debate, see [13] and references therein. However, the effect of the particle size on the PL emission is quite significant. In Fig. 2 the PL from nanoparticle samples with different mean particle diameters is shown. The mean particle diameter is varied between $d = 4.1\,\text{nm}$ and $d = 5.2\,\text{nm}$. This comparably small change in particle size leads to significant shifts in the PL emission energy, from $E \approx 1.4\,\text{eV}$ for the largest particles to about $E = 1.67\,\text{eV}$ for the particles with the smallest diameter. The overall peak shape stays mostly unaffected, except for the sample with the smallest particles, where a stronger high-energy wing is observed. This could be due to the enhanced oscillator strength of the smaller particles, as discussed later in this review. In Fig. 3, the photoluminescence is plotted for three different temperatures. As expected from Varshni's law, one observes a blueshift of the PL emission peak energy with decreasing temperatures. At the same time, however, the intensity exhibits a non-monotonic behaviour: Cooling the sample from 300 to 80 K, the PL intensity increases first, reaches a maximum at $T \approx 80\,\text{K}$ and then decreases again when the temperature is decreased further. This is different from what is observed in most other semiconductor quantum dots or nanocrystals made from direct semiconductors: in such systems, the exciton population increases as the thermal energy of the system is reduced, leading to an increase in the PL intensity with decreasing temperature [14–16]. A systematic study of the temperature dependence of the Si nanoparticle photoluminescence intensity is shown in Fig. 4. It can clearly be seen that the PL intensity maximum is around $T \approx 80\,\text{K}$. At the same time, the PL does not quench for $T \to 0$. Similar results have been obtained for Si nanocrystals embedded in a SiO_2 matrix [3].

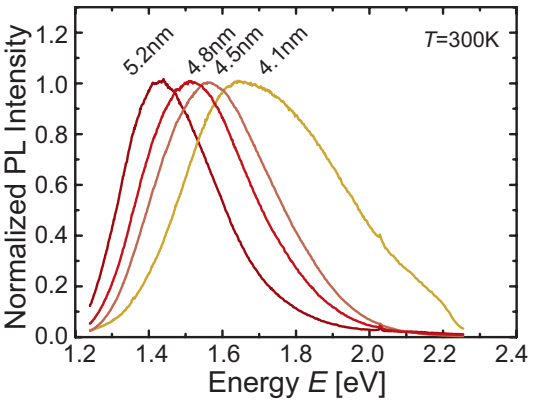

Fig. 2. Room temperature photoluminescence of silicon nanoparticles with different mean particle diameters.

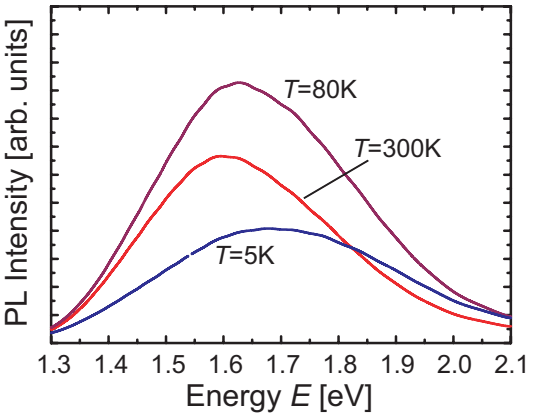

Fig. 3. Photoluminescence of silicon nanoparticles at room temperature, $T = 80\,\mathrm{K}$ and $T = 5\,\mathrm{K}$.

The reason for this behaviour is the excitonic fine structure in the silicon nanoparticles. The left part of Fig. 5 shows the schematic band structure $E(k)$ for the silicon nanoparticles. It should be noted that in this study, only particles with diameters larger than $d = 2.5\,\mathrm{nm}$ are studied, where one can still apply the Bloch equation based band structure model. For smaller clusters, the situation changes and a HOMO/LUMO approach has to be applied [12]. The quantum confinement in the nanoparticles leads to a lifting of the degeneracy of the heavy-hole and the light-hole band at the Γ-point, as the energy shift is inversely proportional to the effective mass. Therefore, for the optical transitions in the silicon nanoparticles one needs to take into account only the conduction band and the heavy-hole band. The conduction band is

s-like, corresponding to an angular momentum component of $J_z^{\mathrm{el}} = \pm 1/2$. The heavy-hole band is p-like and is characterized by an angular momentum component of $J_z^{\mathrm{hh}} = \pm 3/2$. For the formation of excitons, four possibilities exist to align the respective angular momentum components: Two parallel configurations and two antiparallel configuration, leading to a twofold degenerate exciton state with $J_{\mathrm{exc}} = 1$ and another twofold degenerate exciton state with $J_{\mathrm{exc}} = 2$. Because the excitons with $J_{\mathrm{exc}} = 2$ cannot transfer their angular momentum to a single photon with $J = 1$, these exciton states are called "dark excitons" and the other states "bright excitons". Due to the exchange interaction, the degeneracy between the bright and the dark states is lifted, so that the dark states are lower in energy with respect to the bright states by a splitting energy Δ as indicated in the right part of Fig. 5.

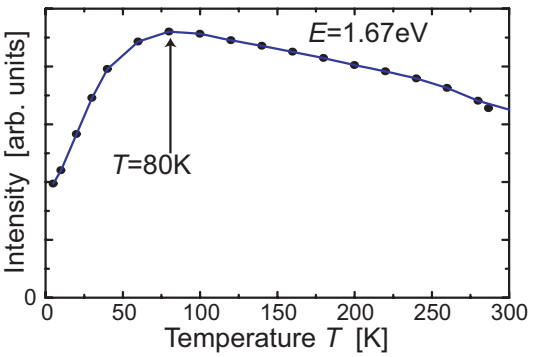

Fig. 4. Photoluminescence intensity of silicon nanoparticles as a function of the temperature.

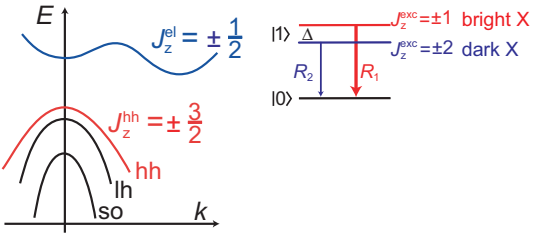

Fig. 5. (*Left*) Schematic band structure for silicon nanoparticles. The quantum confinement leads to a lifting of the degeneracy of the heavy and light hole bands at Γ. (*Right*) Excitonic fine structure.

To study the excitonic fine structure of the silicon nanoparticles in greater detail, one needs to look at the dynamics of the recombination. Therefore, we studied the photoluminescence decay as a function of emission and temperature. As the emission energy scales directly with the particle size, this is equivalent to studying the size dependence of the recombination dynamics. The temperature can be used to change the population of the fine structure of the split states, as will be discussed later. The results of these measurements

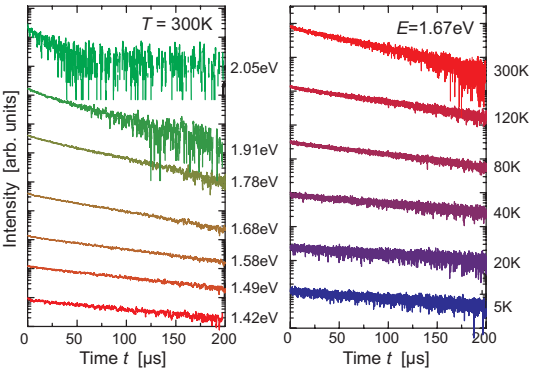

Fig. 6. (*Left*) Photoluminescence decay measured at different emission energies at room temperatures. (*Right*) PL decay at $E = 1.67\,\mathrm{eV}$ for different temperatures.

are shown in Fig. 6. In the left part, the PL decay at $T = 300\,\mathrm{K}$ is shown for different emission energies, corresponding to different particle sizes. As one can see, the PL decay shows a monoexponential behaviour with decay times τ ranging from 40 to 200 µs. This monoexponential decay is indicative of a high degree of crystallinity in the samples used, which suggests that the plasma-based fabrication leads to nanoparticles with better optical properties than those generated, e.g., by photoelectrochemical etching routes, where a stretched exponential decay with a disorder parameter β is reported [17]. The reason for the decrease of PL decay time with decreasing nanoparticle diameter is the increase in phonon-assisted recombinations with decreasing particle size due to the increased electron-phonon interaction in small particles [18]. At the same time, the contributions from the phonon-less transitions also increase due to the enhanced electron-hole wave function overlap [19].

While the PL intensity has a maximum around $T = 80\,\mathrm{K}$, the PL decay times τ_{PL} exhibit a monotonic behaviour: As shown in the right part of Fig. 6 and for more temperatures in the upper part of Fig. 7, τ_{PL} increases with decreasing temperatures.

To isolate the temperature dependence of the radiative recombinations from the total PL decay, one can combine the information from the temperature dependence of the photoluminescence intensity $I(T)$ with the temperature

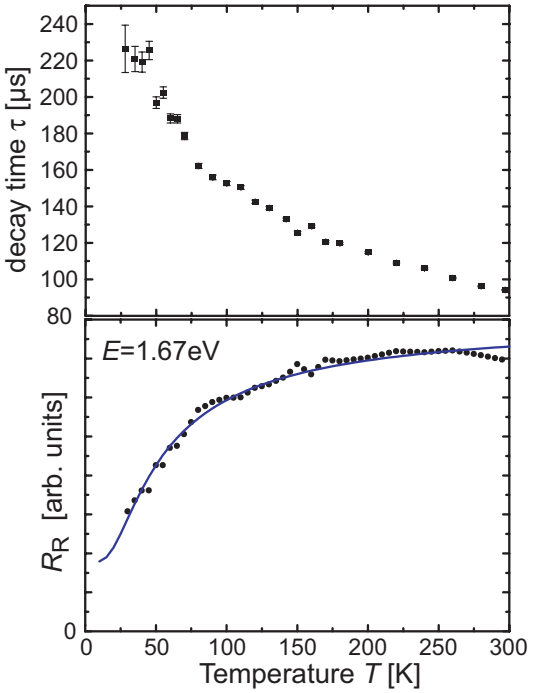

Fig. 7. (*Upper part*) Measured PL decay times. (*Lower part*) Temperature dependence of the radiative recombinations.

dependence of the PL decay rate $R_{\mathrm{PL}} = 1/\tau_{\mathrm{PL}}$. The PL decay rate consists of the radiative and the non-radiative recombination rate:

$$R_{\mathrm{PL}} = R_{\mathrm{R}} + R_{\mathrm{NR}}.$$

The intensity is proportional to the quantum efficiency η:

$$I \propto \eta = \frac{R_{\mathrm{R}}}{R_{\mathrm{R}} + R_{\mathrm{PL}}}$$

Therefore, the product of intensity and PL decay rate is proportional to the radiative recombination rate alone: $\rightarrow I(T) \cdot R_{\mathrm{PL}} \propto R_{\mathrm{R}}$. The result of this analysis is shown in the lower part of Fig. 7. The circles represent data points, while the solid line stems from the model described below. One can see, that the radiative recombination rate decreases as the temperature is reduced, contrary to what is observed to direct semiconductor quantum dot/nanocrystal systems such as InAs quantum dots or CdSe/CdS nanocrystals.

The fact that the radiative recombination rate *decreases* towards lower temperatures suggests that in this regime the dark states play a dominant role. The fact, that the dark state is lower in energy than the bright state (see

Fig. 5) is a hint that the excitons can thermalize into the lower (dark) state before recombining. In other, direct gap semiconductor quantum systems such a thermalization between the bright and the dark state is not possible as the exciton lifetimes are much shorter, typically in the range of few nanoseconds. In the case of silicon nanoparticles however, the lifetimes are much longer, suggesting that the excitons can scatter and a thermal equilibrium between the dark and the bright state is established. Therefore, we can use a thermal distribution of the states to calculate the total radiative recombination rate R_{R} as a function of the temperature using only the parameters R_1 and R_2 for the individual recombination rates from the bright and the dark state, respectively, and the exchange interaction energy Δ. The radiative recombination rate is then given by:

$$R_{\mathrm{R}} = \frac{2R_2 + 2R_1 \cdot \exp\left(-\frac{\Delta}{k_{\mathrm{B}}T}\right)}{2 + 2 \cdot \exp\left(-\frac{\Delta}{k_{\mathrm{B}}T}\right)}$$

However, due to the fact that the intensity is only proportional but not equal to the quantum efficiency, only the temperature dependence of the radiative recombination rate $R_{\mathrm{R}}(T)$ is known, but not the absolute values. Therefore, by fitting the above equation to the data points in the lower part in Fig. 7, we can only obtain the ratio of R_1/R_2 and not the individual values. Moreover, we can deduce the exchange interaction energy Δ from the above model. Fitting the data to the above equation yields an exchange energy of $\Delta = 5.8\,\mathrm{meV}$ and a ratio of bright state/dark state recombination rate of $R_1/R_2 = 8$. The first value is significantly higher than the value for bulk silicon, for which $\Delta = 140\,\mu\mathrm{eV}$ has been reported [20]. However, the splitting energy is mostly given by short-range exchange interaction, which is enhanced in confined systems [21]. The result for the ratio between the bright and dark state recombination rate is more surprising. As discussed before, one expects the dark exciton states to be optically inactive due to the total angular momentum conservation rule. In such a case, however, one should obtain $R_1/R_2 \to \infty$ as the recombination from the dark states should be $R_2 \approx 0$. Our experiments, however, strongly suggest that the dark state recombination plays an important role for the PL at low temperatures. Indeed, applying the above model, we can even estimate that for $T < 40\,\mathrm{K}$ the luminescence rate from the dark excitons is larger than the one from the bright states [8] due to the preferential occupation of the lower dark state over the energtically higher bright state. To check these findings, we analyzed the photoluminescence decay as a function of the emission energy for different temperatures. The results are plotted in the upper part of Fig. 8. While for temperatures $T > 40\,\mathrm{K}$ we find the expected decrease in PL decay time τ_{PL} with increasing emission energy (decreasing particle size), the results for $T < 40\,\mathrm{K}$ show an entirely different behaviour: In this regime, the measured PL decay times are nearly independent of particle size and temperature and have a nearly constant value of $\tau_{\mathrm{PL}} \approx 200\,\mu\mathrm{s}$. The reason for this is a non-radiative decay mechanism which limits all measurable decay times.

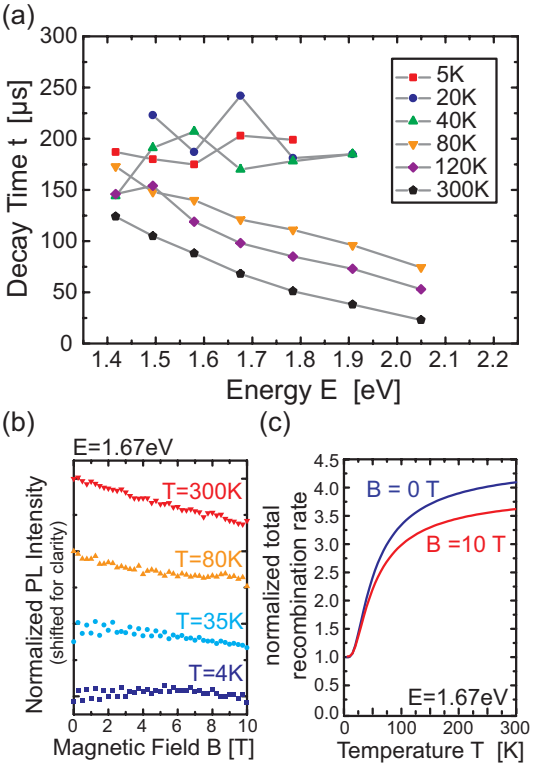

Fig. 8. (**a**) PL decay times for different temperatures. (**b**) PL intensity as a function of the magnetic field for different temperatures. (**c**) Calculated recombination from the dark and the bright state based on a thermal distribution between the states.

In principle, we would expect also for the dark excitons an increase in the recombination rate with decreasing particle size.

Another test for the above discussed model is to investigate the PL intensity at different temperatures as a function of the magnetic field. The magnetic field causes a mixing of the dark and the bright state. This should lead to a significant effect at higher temperatures, where both states are occupied, and a change in the recombination rate of the bright exciton should have a greater impact. At low temperatures, where the excitons are mostly in the dark state, one only expects a small effect on the intensity. The results of the corresponding measurements are shown in the lower part of Fig. 8. Indeed, one finds that for larger temperature the PL intensity decreases, when the magnetic field is increased. In the same manner, the intensity is nearly independent of the magnetic field at low temperature.

The above measurements gives an excellent estimate for the non-radiative recombination time τ_{NR} in this system, a quantity, which is always present

in semiconductor quantum systems, but usually difficult to access experimentally. Using these results, we can now immediately calculate the *radiative* recombination times from the measured PL decay times τ_{PL}: $\tau_{\mathrm{R}}^{-1} = \tau_{\mathrm{PL}}^{-1} - \tau_{\mathrm{NR}}^{-1}$. From this, we can then determine the oscillator strength $f_{\mathrm{osc}}(\omega)$ that describes the strength of an optical transition:

$$f_{\mathrm{osc}}(\omega) = \frac{2\pi\varepsilon_0 mc^3}{e^2 n\omega^2}\frac{1}{\tau_{\mathrm{R}}}$$

In the above equation, n is the refractive index and $m = m_e + m_h$ is the exciton mass in the weak confinement regime, given by the sum of the individual masses $m_e = 0.19m_0$ and $m_h = 0.286m_0$ [22, 23].

The results of the above calculations are shown in Fig. 9 together with the radiative recombination times derived via the above route. The oscillator strengths found for the present silicon nanoparticles are in the range of $f \approx 10^{-5}$ for emission energies between 1.4 and 2.1 eV. The oscillator strength increases with increasing emission energy/decreasing particle size. This is due to the increased localization of the electron and hole wavefunctions in the nanocrystals, leading to larger dipole matrix elements and thus larger oscillator strength. These results are in excellent agreement with recent theoretical results obtained using the tight-binding method [12].

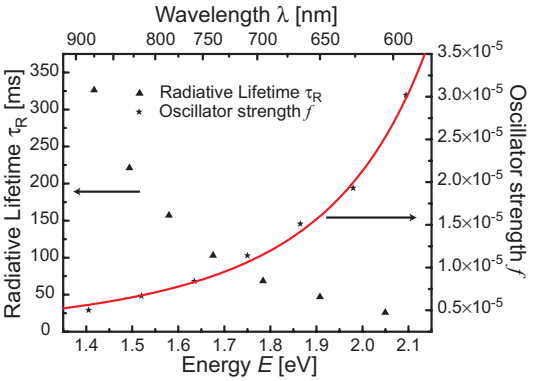

Fig. 9. PL decay and oscillator strength over the PL emission energy.

Using the values for both the radiative and non-radiative recombination rates, it is also possible to estimate the quantum efficiency for the optical transitions in these particles. The quantum efficiency is given by:

$$\frac{\tau_{\mathrm{R}}^{-1}}{\tau_{\mathrm{R}}^{-1} + \tau_{\mathrm{NR}}^{-1}}$$

Using this technique, one obtains quantum efficiencies between $\eta = 34\%$ and $\eta = 86\%$, where the quantum efficiency increases with decreasing particle

sizes. It is interesting to point out that this method does not rely on either an Ulbricht sphere or the use of a calibrated standard sample, but just on the time-resolved PL measurements. Similar values for silicon nanoparticles have also been reported by other groups [6, 24].

4 Conclusion

In the present paper, we have reviewed some recent results on the photoluminescence properties of silicon nanoparticles. We find that the excitonic fine structure can be used to describe the experimentally found temperature dependence of the stationary and dynamic photoluminescence results. While at room temperature, the photoluminescence is clearly governed by recombinations from the energetically higher bright states, at about $T = 40\,\mathrm{K}$ the dark states start to dominate and govern the low temperature photoluminescence properties. The reason for this is the ability of the exciton system to thermalize due to the large exciton lifetimes in this system. By analyzing the PL decay results, we can also demonstrate that the behaviour of bright and dark states is clearly different. From these results we can deduce the non-radiative lifetime, which allows us finally to experimentally deduce the osciallator strength. The obtained values are in excellent agreement with theory.

5 Acknowledgments

This work was supported by the Deutsche Forschungsgemeinschaft (DFG) via grant "SFB 445-Nanoparticles from the gas phase" and "GRK 1240-Nanotronics".

References

1. L. Canham, Appl. Phys. Lett. **57**, 1046 (1990).
2. J. Linnros, N. Lalic, A. Galeckas, and V. Grivickas, J. Appl. Phys. **86**, 6128.
3. M. L. Brongersma, P. G. Kik, A. Polman, K. S. Min, and H. A. Atwater, Appl. Phys. Lett. **76** 351 (2000).
4. J. Heitmann, F. Müller, M. Zacharias, and U. Gösele, Adv. Mater. **17**, 795 (2005).
5. G. Ledoux, O. Guillois, D. Porterat, C. Reynaud, F. Huisken, B. Kohn, and A. Paillard, Phys. Rev. B **62**, 15942 (2000).
6. L. Mangolini, E. Thimsen, and U. Kortshagen, Nano Lett. **5**, 655 (2005).
7. C. Meier, A. Gondorf, S. Lüttjohann, and A. Lorke, J. Appl. Phys. **101**, 103112 (2007).
8. S. Lüttjohann, C. Meier, M. Offer, and H. Wiggers, Eurphys. Lett. **79**, 37002, (2007).

9. L. Pavesi, L. DalNegro, C. Mazzoleni, G. Franzo, and F. Priolo, Nature **408**, 440 (2000).
10. R. J. Walters, G. I. Bourianoff, and H. A. Atwater, Nat. Mater. **10**, 1038 (2005).
11. J. Knipping, H. Wiggers, B. Rellinghaus, P. Roth, D. Konjhodzic, and C. Meier, J. Nanosci. Nanotechnol. **4**, 1039 (2004).
12. F. Trani, G. Cantele, D. Ninno, and G. Iadonisi, Phys. Rev. B **72**, 075423 (2005).
13. S. Godefroo, M. Hayne, M. Jivanescu, A. Stesmans, M. Zacharias, O. I. Lebedev, G. van Tendeloo, and V. V. Moshchalkov, Nat. Nantechnol. **10**, 1038 (2008).
14. J. C. Kim, H. Rho, L. M. Smith, H. E. Jackson, S. Lee, M. Dobrowolska, and J. K. Furdyna, Appl. Phys. Lett. **75**, 214 (1999).
15. Y. G. Kim, Y. S. Joh, J. H. Song, K. S. Baek, S. K. Chang, and E. D. Sim, Appl. Phys. Lett. **83**, 2656 (2003).
16. E. C. Le Ru, J. Fack, and R. Murray, Phys. Rev. B **67**, 245318 (2003).
17. L. Pavesi and M. Ceschini, Phys. Rev. B **48**, 17625 (1993).
18. D. Kovalev, H. Heckler, M. Ben-Chorin, G. Polisski, M. Schwartzkopf, and F. Koch, Phys. Rev. Lett. **81**, 2803 (1998).
19. M. S. Hybertsen, Phys. Rev. Lett. **72**, 1514 (1994).
20. J. C. Merle, M. Capizzi, P. Fiorini, and A. Frova, Phys. Rev. B **17**, 4821 (1978).
21. D. H. Feng, Z. Z. Xu, T. Q. Jia, X. X. Li, and S. Q. Gong, Phys. Rev. B **68**, 035334 (2003).
22. J. B. Xia, Phys. Rev. B **40**, 8500 (1989).
23. A. D. Yoffe, Adv. Phys. **42**, 173 (1993).
24. D. Jurbergs, E. Rogojina, L. Mangolini, and U. Kortshagen, Appl. Phys. Lett. **88**, 233116 (2006).